Available online at www.sciencedirect.com

ScienceDirect

Journal of the European Ceramic Society 34 (2014) 2823–2831

www.elsevier.com/locate/jeurceramsoc

Evidence of optimal interfaces in bio-inspired ceramic-composite panels for superior ballistic protection

Stefano Signetti [a], Nicola M. Pugno [a,b,c,*]

[a] *Laboratory of Bio-Inspired and Graphene Nanomechanics, Department of Civil, Environmental and Mechanical Engineering, University of Trento, Via Mesiano 77, I-38123 Trento, Italy*

[b] *Centre for Materials and Microsystems, Fondazione Bruno Kessler, Via Sommarive 18, I-38123 Povo (Trento), Italy*

[c] *School of Engineering and Materials Science, Queen Mary University of London, Mile End Road, E1 4NS, London, UK*

Received 15 November 2013; accepted 19 December 2013
Available online 4 February 2014

Abstract

Ceramic-composite panels are acknowledged to provide effective impact protection even against small fragments and armour piercing projectiles. Nature shows similar solutions, coupling an hard face and soft backing layers, in dermal animal armours for protection against predators. Finite element simulations of impact on ceramic-composite panels, to evaluate their energy absorption capability, are presented. The influence of key parameters, like interface strength and friction, on ballistic limit is studied. We find that a proper set of interface parameters is able to maximize the specific energy absorption of the panel: although this optimum is variable case by case depending on projectile penetrability and target configuration, general guidelines are provided. Oblique impact results in a higher ballistic limit also thanks to projectile change in trajectory, providing interesting spots for future developments. Numerical results are compared with experimental data from literature and forecasts of analytical models.

Keywords: Impact; Ceramic-composite panels; Energy absorption; Oblique impact; Finite element simulations

1. Introduction

Laminated composite materials are widely employed in protective armours, automotive and aerospace applications: these homogeneous panels have their weak point in small and high penetrating fragments and armour piercing (AP) projectiles. Hard faced ceramics with a multilayered composite backing are widely used in order to solve these problems, for example, in protective body armours. On these heterogeneous plates, impactors are first blunted and weared down by the exterior hard ceramic which also spreads the load over a larger area; then the composite tough backing[1–5] deforms and absorbs the residual kinetic energy of the decelerated and damaged fragment; the backing also delays and mitigates the initiation of tensile failure in the ceramic and it is capable to catch both ceramic and impactor fragments, preventing them to constitute further injury. This solution can be found also in nature, for example in *Arapaima gigas* dermal armour, whose scales are made up of an external hard mineral layer on a multilayered collagen backing.[6]

The optimum balance between lightness, thickness, performance, and economic requirements is a challenging engineering task. Ceramics are lighter with respect to traditional monolithic hard-steel panels, while comparable in stiffness, hardness and compressive strength. However, they are characterized by a higher density (about a factor of two) with respect to composite materials. Thus, their use has to be carefully balanced and limited in lightweight applications like, for instance, spacecraft or human body protection from micrometeorites and space debris.

Alumina (Al_2O_3), Boron Carbide (B_4C) and Silicon Carbide (SiC) are some of the most widely employed ceramics in the sector. For the backing, polyetilene- and aramid-based tough fibres are arranged in woven or unidirectional (UD) textiles within a polymer thermoplastic or thermoset matrix (epoxy or vinylester resins): they can range from traditional ones, like Kevlar® (aramid), and more recent like Dyneema® (UHMWPE)[7] or Twaron® (aramid).[8] The main advantage of composites is that that their properties can be tailored on the requirements for a specific application. High specific strength, specific stiffness

* Corresponding author at: Laboratory of Bio-Inspired and Graphene Nanomechanics, Department of Civil, Environmental and Mechanical Engineering, University of Trento, Via Mesiano 77, I-38123 Trento, Italy.
Tel.: +39 0461 282525; fax: +39 0461 282599.
E-mail address: nicola.pugno@unitn.it (N.M. Pugno).

0955-2219/$ – see front matter © 2014 Elsevier Ltd. All rights reserved.
http://dx.doi.org/10.1016/j.jeurceramsoc.2013.12.039

and toughness make them an obvious choice for aerospace vehicles; the resistance against unkind environments (e.g. corrosive, UV, extreme temperatures, etc.), enhances the robustness of the structure. A measure of the fibres performance against ballistic impact was provided by Cunniff[9] for flat targets hit by cylindrical projectiles, and was defined as the product of the fibres specific toughness by the strain wave velocity.

The design and the performance evaluation of composite panels undergoing ballistic impact require the understanding of material properties under high-velocity impact conditions. Recht and Ipson[10] proposed a relatively simple analytical model, based on energy conservation laws, able to determine ballistic curves to fit experimental results. In this model the final velocity V_f of the impactor is given, as a function of its initial velocity V_0, by:

$$V_{\mathrm{f}} = q\left(V_0^p - V_B^p\right)^{1/p} \tag{1}$$

where V_B is the target ballistic limit, p a fitting parameter, usually equal to 2 in case of rigid projectiles and target resistance independent to impactor velocity, and q a coefficient depending on model assumption (e.g.: $q = 1$ if assuming that dissipation is only due to target deformation, and no projectile damage is considered). A comparison between experimental ballistic curves and Eq. (1) can be found in Ref. 11 showing that this model can apply with a good level of approximation for the estimation of the final velocity, both for isotropic and heterogeneous composite material.

Espinosa et al.[12] investigated the response of multilayered ceramic–steel targets under high-velocity impact through finite element simulations. A multiple-plane microcracking model to describe the inelastic constitutive behaviour of ceramics under severe damage was implemented into a finite element code. Their analyses showed that the penetration process is highly dependent on the multilayered configuration (stacking sequence) and the target structural design (geometry and boundary conditions), rather than on the type and properties of the ceramic material. In addition the erosion parameter in simulations, to which the residual damage strength is related, plays a key role in predicting the interaction of the penetrator in the target: thus, a coupled experimental and numerical study is found to be necessary in a meaningful ceramic-composite armour design.

Hetherington et al.[13,14] developed an analytical model for the analysis of two-component composite armours subjected to normal and oblique impact. They observed that, circular contours of constant deformation which occur in backing plates under normal impact, tends to be elliptical for oblique strike. They assumed that the projectile tip deforms into an ellipse as it impacts the front face of the ceramic under the oblique impact. It was found that an inclined ceramic composite armour plate is more effective, on a thickness basis, than one arranged perpendicular to the line of impact; parallel the ballistic limit velocity increases with obliquity. This model is reported in Ref. 15.

Considering the cost related to the ceramic and composite materials used in ballistic experiments, the need for developing accurate predictive simulation tools becomes more important. Large simulation sensitivity campaigns would let the understanding of the influence of each considered parameter, leading into the design of the optimal solution that couples toughness maximization and weigh reduction. Analytical modelling for the evaluation of impact behaviour of composite targets[16,22] generally assumes the laminate resistance σ as a quadratic function of the impactor istantaneous velocity V, taking into account strain rate effects, $\sigma = \sigma(V, V^2)$. Since the backing layers, due to impactor deceleration, progressively face a lower velocity, the specific absorbed energy E_{abs} for each ply is expected to decrease as the number of layers N, i.e. the areal density of the plate, increases:

$$\frac{E_{\mathrm{abs}}}{N} \propto N^{\alpha} \tag{2}$$

with $\alpha < 0$. However, this is usually in contrast with experimental tests which show that generally the exponent α can be positive. Jacobs and Van Dingenen[23] showed how the scaling of Eq. (2) can invert from soft to hard (pressed) panel: however, in the study it is not provided a formal explanation of the trend. The observation of scalings of energy absorption and the understanding of related mechanisms could lead into optimized panels against high-strain and strain-rate loads.

Our study focuses on these trends in order to find if and how the failure mechanism of ceramic-composite panels could be enhanced in order to maximize dissipation. The outcomes would be extensible in general to other typologies of multilayered structures. The effect of oblique impact on the ballistic limit is also studied. These scopes require advanced finite element models with proper material constitutive laws in order to catch the real dynamics of impactor–armour interaction and to find effective ways of developing optimized solutions. This work presents a numerical model for ballistic impact simulations in hybrid ceramic-fibre reinforced composite armours. The explicit non-linear finite element solver LS-DYNA®[24,25] was used.

2. Modelling of impact

Basing on an energetic approach for modelling impacts, as widely used in literature,[16–23] the variation of projectile kinetic energy in penetrating the plate must balance the amount of dissipated energy (E_{abs}) in the damaged volume of the target, which is assumed to be cylindrical and, defined by the projectile radius R and the plate thickness t. Thus, the following relation can be written:

$$\tfrac{1}{2}mV_0^2 - \tfrac{1}{2}mV_f^2 = \sigma\pi R^2 t \tag{3}$$

where m is the mass of the projectile, V_0 and V_f the initial and final velocity of the impactor respectively and σ the ultimate compressive strength of the material. Assuming a rigid projectile, Eq. (3) yields Eq. (1) for $q = 1$ and $p = 2$. A more realistic approach consists in considering the velocity as a quadratic function of the istantaneous impact velocity V; for each layer it can be assumed:

$$\sigma = \sigma_0\left(a_0 + a_1 kV + a_2 k^2 V^2\right) \tag{4}$$

where a_0, a_1, a_2 are parameters depending on material behaviour and impactor geometry according to Ref. 21, σ_0 is the material

compressive strength at the reference strain-rate, and $k = \sqrt{\gamma/\sigma_0}$ the square root of the ratio between the undeformed target density γ and the nominal material strength. Extending Eq. (3) to a sequence of n layers, the final velocity after the passage through the (i-1)-th layer would be the initial velocity seen by the i-th one ($V_0 = V_{i\text{-}1}$) and then $V_f = V_i$. Introducing then the strength dependency given by Eq. (4) and assuming $a_1 = 0$ (generally valid for high-velocity impacts), the energy balance can be easily integrated and the velocity V_i after the passage through the considered i-th layer obtained:

$$V_i = \sqrt{\left(\frac{\exp\left(-t_i \frac{2a_{2,i}k_i^2 \pi \sigma_i R^2}{m}\right)\left(a_{0,i} + a_{2,i}k_i^2 V_{i-1}^2\right) - a_{0,i}}{a_{2,i}k_i^2} \right)}, \tag{5}$$

valid until the expression under the root is positive, unless the impactor residual velocity is equal to zero, so it is stopped. Summing the decelerating contribution of each ply given by Eq. (5), the final velocity of the impactor can be obtained. Moreover, the mutual effect between layers under deformation can not be caught since Eq. (5) is independent from the distance s between adjacent plies.

Parallel, three-dimensional finite element models of projectile and target were built up using LS-DYNA® finite element code,[24,25] with high non-linear solving capabilities. The projectile was modelled at this stage as rigid body. The thickness ratio of the two-components composite plate was decided upon the work of Hetherington,[26] where it was concluded upon experimental results that the optimum ratio in order to maximize the energy absorption, i.e. the plate ballistic limit, is given by the following relation:

$$\frac{t_1}{t_2} \approx 4 \cdot \frac{\rho_2}{\rho_1} \tag{6}$$

where t_1 and t_2 are the ceramic and composite thicknesses respectively, ρ_1 and ρ_2 the corresponding material densities. Fig. 1 shows the typical finite element model for impact simulation used in our studies. Only a quarter of circular plate with proper boundary conditions was modelled for studying plate energy absorption, half a plate for studying oblique impact due to symmetry considerations. The minimum in-plane dimensions of the target representative part were decided upon the fact that both experiments and numerical simulations evidence that during high-velocity impact the radius of the load-influenced area does not exceed six times the radius R of the impacting object.

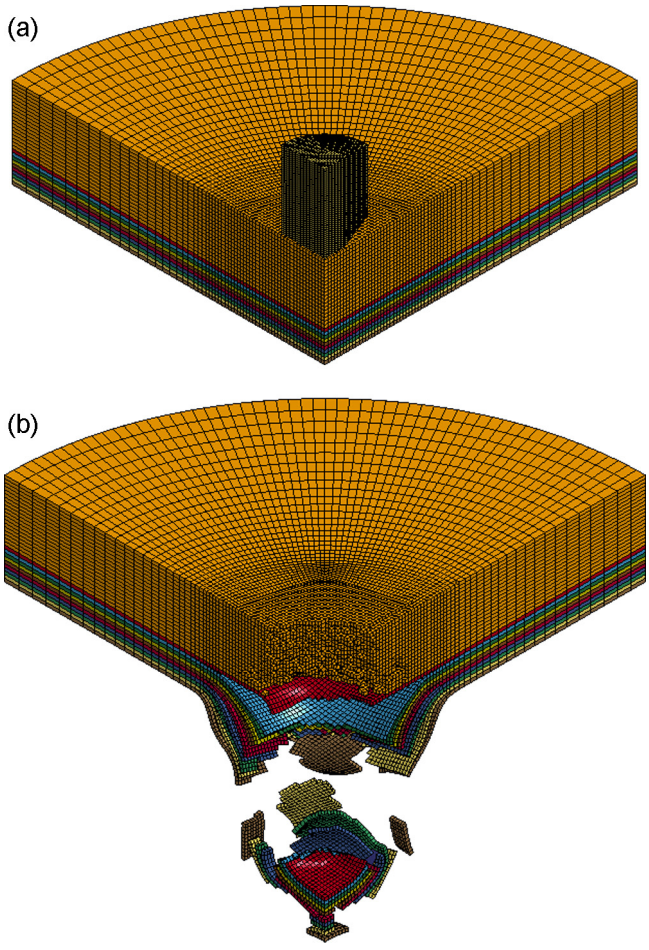

Fig. 1. (a) Finite element model of impact on ceramic-composite panel and (b) example of ceramic-composite target deformation after complete penetration ($t_1 + t_2 = 3.8 + 2$ mm, $V_0 = 700$ m/s, $V_f = 608$ m/s).

The ceramic was implemented through the Johnson–Holmquist JH-II material model (MAT_110),[27] able to describe the response of brittle materials subjected to large deformation at high strain rates. Under quasi-static loading

Table 1
Ceramic material input constants of boron carbide (B_4C) for LS-DYNA® *MAT_110.[28]

Density [kg/m^3]	G [GPa]	A	B	C	M	N
2510	197	0.927	0.7	0.005	0.85	0.67
EPSI	T [GPa]	SFMAX	HEL	PHEL	BETA	
1.0	0.26	0.2	19	8.71	1.0	
D1	D2	K1 [GPa]	K2 [GPa]	K3 [GPa]	FS	
0.005	0.5	233	−593	2800	0	

G – elastic shear modulus; A – intact normalized strength parameter; B – fractured normalized strength parameter; C – strength parameter (for strain rate dependence); M – fractured strength parameter (pressure exponent); N – intact strength parameter (pressure exponent); EPSI – reference strain rate; T – maximum tensile pressure strength; SFMAX – maximum normalized fractured strength; HEL – Hugoniot elastic limit; PHEL – pressure component at the Hugoniot elastic limit; BETA – fraction of elastic energy loss converted to hydrostatic energy; D1 – parameter for plastic strain to fracture; D2 – parameter for plastic strain to fracture (exponent); K1 – first pressure coefficient (equivalent to the bulk modulus); K2 – second pressure coefficient; K3 – third pressure coefficient; FS – failure criteria.

Table 2
Kevlar-epoxy composite backing properties for LS-DYNA® *MAT_58. For the detailed meaning of each parameter, see Ref. 25.

KEVLAR						
Density [kg/m^3]	EA [GPa]	EB [GPa]	EC [GPa]	PRBA	TAU1 [GPa]	GAMMA1
2130	164	164	18	0.0	0.0	0.0
GAB [GPa]	GBC [GPa]	GCA [GPa]	SLIMT1	SLIMC1	SLIMT2	SLIMC2
18	18	18	0.05	0.50	0.05	0.50
E11C	E11T	E22C	E22T	GMS		
0.35	0.1	0.35	0.1	0.25		
XC [GPa]	XT [GPa]	YC [GPa]	YT [GPa]	SC [GPa]		
0.950	0.500	0.950	0.500	0.200		
EPOXY RESIN						
Density [kg/m3]	EA [GPa]	EB [GPa]	EC [GPa]	PRBA	TAU1 [GPa]	GAMMA1
900	0.5	0.5	0.5	0.34	0.0	0.0
GAB [GPa]	GBC [GPa]	GCA [GPa]	SLIMT1	SLIMC1	SLIMT2	SLIMC2
0.187	0.187	0.187	0.5	0.5	0.5	0.5
E11C	E11T	E22C	E22T	GMS		
0.350	0.05	0.350	0.05	0.025		
XC [GPa]	XT [GPa]	YC [GPa]	YT [GPa]	SC [GPa]		
0.400	0.02	0.400	0.02	0.0075		

EA – Young's modulus in longitudinal direction (A); EB – Young's modulus in transverse direction (B); EC – Young's modulus in normal direction (C); PRBA – Poisson's ratio; TAU1 – stress limit for the non-linear part of shear stress vs. shear strain curve; GAMMA1 – strain limit for the non-linear part of shear stress vs. shear strain curve; GAB – shear modulus in AB plane; GBC – shear modulus in BC plane; GCA – shear modulus in CA plane; SLIMT1 – stress limit factor after the stress maximum (fibre tension); SLIMC1 – stress limit factor after the stress maximum (fibre compression); SLIMT2 – stress limit factor after the stress maximum (matrix tension); SLIMC2 – stress limit factor after the stress maximum (matrix compression); E11C – strain at longitudinal compressive strength; E11T – strain at longitudinal tensile strength; E22C – strain at transversal compressive strength; E22T – strain at transversal tensile strength; GMS – strain at shear strength; XC – longitudinal compressive strength; XT – longitudinal tensile strength; YC – transversal compressive strength; YT – transversal tensile strength; SC – shear strength.

conditions ceramics may be assumed as elastic-brittle materials; however, when high strain rates are involved (like in ballistic impacts) the post-yield response of the ceramic becomes significant in evaluating its behaviour and then may have non negligible influence on ballistic limit. The model allows for progressive damage, taking into account residual material strength and compressive bulking. The ceramic component was constituted in our case by boron carbide (B_4C): in Table 1 the input material constant are reported; these were available in literature[28] and calibrated through experimental tests.

For the Kevlar® composite backing (Table 2), an orthotropic material model (MAT_58) was used, which implements a linear-elastic branch followed by a non-linear post peak softening behaviour: the residual strength in compression, tension and shear can be defined as a fraction of the maximum material stress (defined by the SLIM factors). The equations which define the

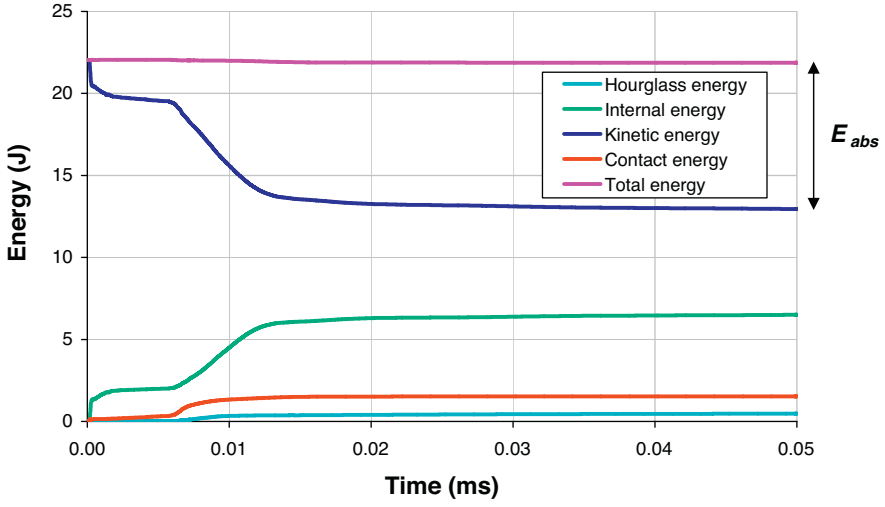

Fig. 2. Energy balance of one of the performed simulations. The sum of internal, contact (sliding interface) and hourglass energies represents the amount of energy absorbed at each time by the plate (E_{abs}). The values refer to the quartered model.

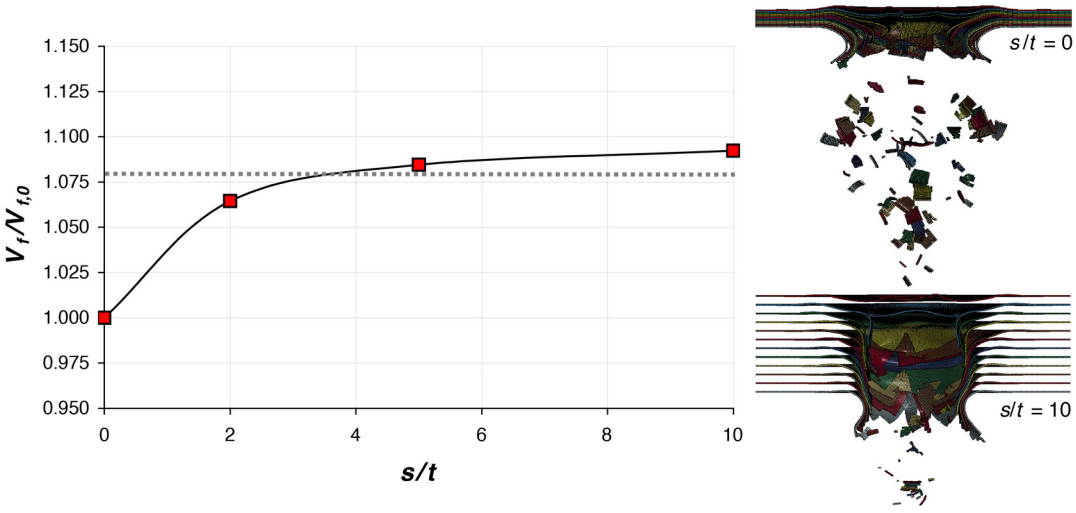

Fig. 3. Residual velocity variation with the interlayer distance s. The dashed line represents the output value given by Eq. (5).

failure criteria are presented in detail in the paper by Schweizerhof et al.[29] The composite material model was implemented in the layered thick shell (TSHELL) element, coupled with a user defined integration rule. This method, more refined than simply using the smeared properties of the ply obtained by a rule of mixture, assigns to each through-thickness integration point the corresponding material (fibre or matrix) properties and constitutive behaviour according to the volumetric fraction of the laminate.

The ceramic target and impacting fragment were modelled with under-integrated solid elements. Hourglass (spurious mode) control was set. The energy balance of one of the performed simulations (Fig. 2) confirms the effectiveness of the built model, as regards contact modelling, material behaviour, and element performance. Hourglass (spurious modes) energy is within the 15% of total internal energy, value that is generally acknowledged for not affecting overall response of the system.

3. Energy absorption under ballistic impact

To first understand the role that layer interaction plays in the resistance mechanism under ballistic impact, several target with

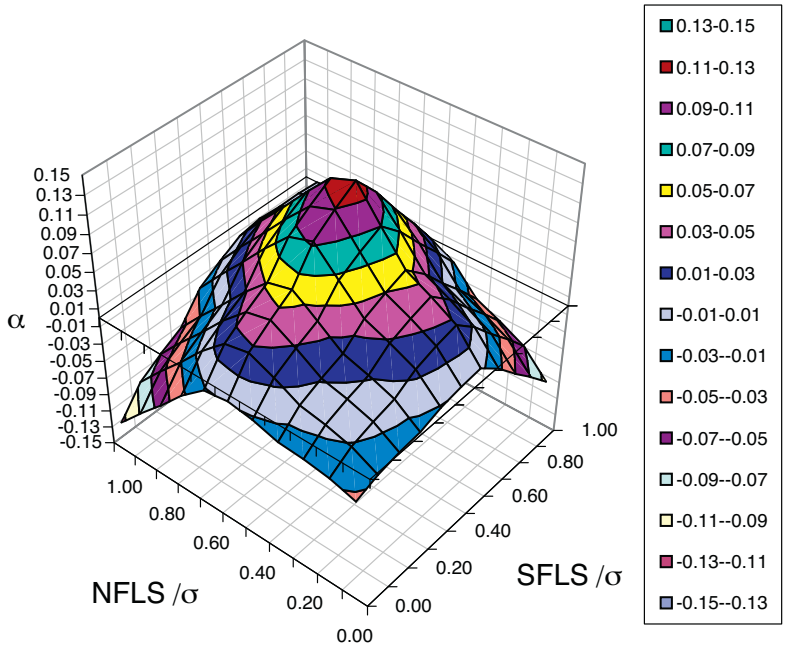

Fig. 4. Influence of delamination strength parameters on specific energy absorption (α exponent), for given inter-laminar friction ($\mu_S = 0.15$, $\mu_D = 0.12$), impactor velocity and shape. The interface normal failure stress (NFLS) and shear failure stress (SFLS) are normalized with respect to single ply resistance σ. The best response arises when both parameters reach approximately one half of laminate peak stress. Too high values of these quantities provide "punch shear" failure (i.e. tends to dissipation by volume, $E_{abs} = \sigma\pi R^2 t \Rightarrow \alpha \leq 0$).

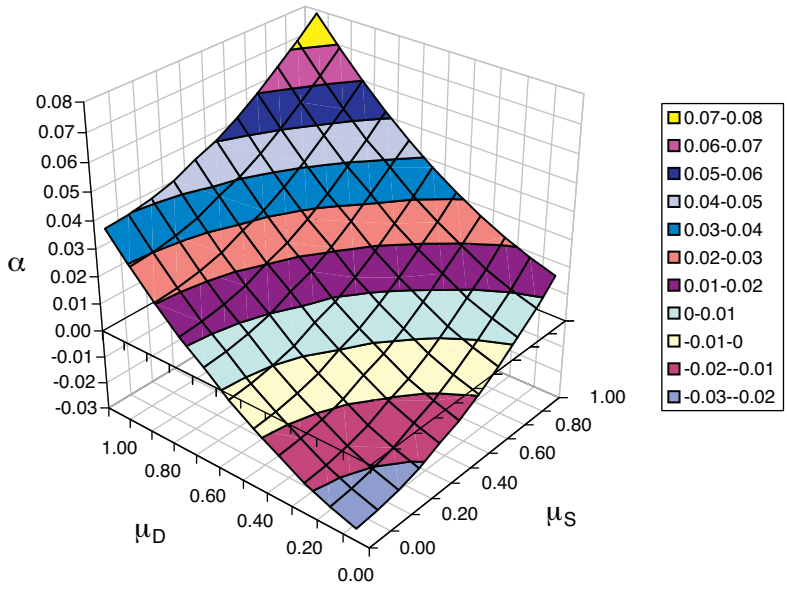

Fig. 5. Influence of the static (μ_S) and dynamic (μ_D) coefficient of friction on the scaling exponent α of specific absorbed energy.

equity of materials and stacking sequence but different distance in between the layer were performed; in this way, any difference in the behaviour is a function of the mere stacking distance *s*, set up for each configuration as a multiple of the each composite ply thickness. In Fig. 3 the variation of residual velocity after penetration with the distance between layers is shown. The distance *s* is normalized with respect to the thickness *t* of the single ply, assumed to be the same for all layers. The absorbed energy decreases as the distance between layer increases, showing that when layers are packed together they are able to work in synergy enhancing performances: when the distance between the layers tends to be significant (almost over 10 times *t*), there is saturation in the trend of residual velocity (and so of the absorbed energy). Since the impactor is modelled as rigid body, the decrement of absorbed energy means a decrease in the internal energy of the plate.

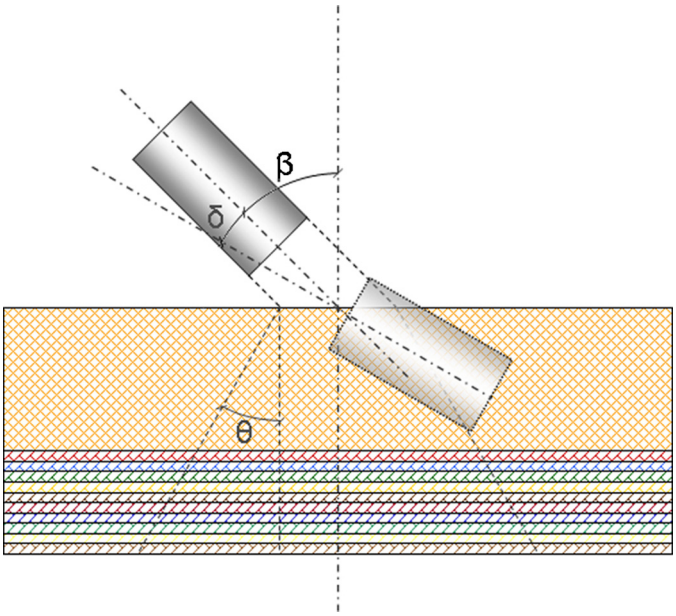

Fig. 6. Scheme of oblique impact configuration on ceramic-composite armour. The damaged zone defined by θ and the possible deviation of the projectile δ from the initial obliquity β are shown.

Since the stacking distance between ceramic and composite layers is seen to be important for overall deformation behaviour under impact, the effect of interface parameter was then studied. In fact, the discrepancy between the energy absorption provided by the energy based analytical model and experimental results (see as example Ref. 23) is intuitively imputable to all those effects that are not considered in the energy balance: the most important are delamination and mechanical interaction between deforming layers. A campaign of simulation was performed in order to assess the influence on interface parameter on overall target behaviour and then on the amount of dissipated energy. The main parameters of interest which define adhesive property are, for the specific contact algorithm implemented in the model: the normal failure stress (NFLS, correlable with Mode I crack opening), the shear failure stress (SFLS, Mode II), and friction.

Fig. 4 shows the dependence of the α exponent to interface strength parameters, with equity of impactor characteristics, velocity and interlaminar friction. An optimum is found. Starting from null interlaminar resistance, both in the in-plane and out-of-plane directions, the increase in delamination strength let the layers to work better. Beyond a certain value, depending on material stiffness, on the stiffness ratio between layers and on the impactor energy and penetrability, the failure mode tends to "punch shear" collapse and the α exponent decreases again and can return negative. The trend is slightly more sensitive to shear adhesive strength. It must be underlined that the failure mode is extremely dependent on the impactor velocity: punch shear

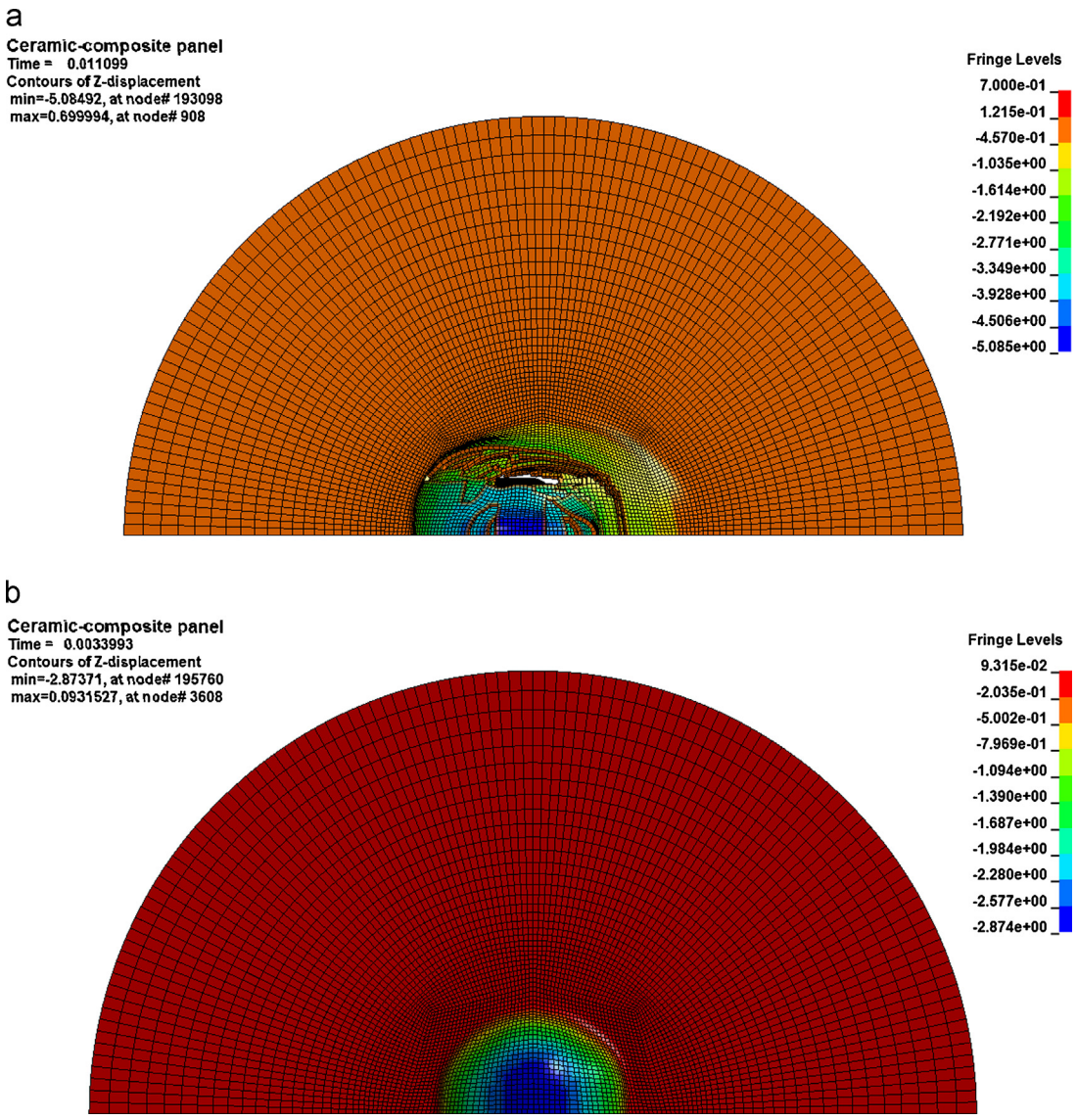

Fig. 7. Back view of the ceramic-composite panel with visualization of projectile imprint through contour of normal displacement: (a) oblique impact ($\beta = 60^\circ$) with elliptical imprint; (b) normal impact with circular imprint.

failure may occur also for low values of interface strength when the impactor is characterized by high penetrability; thus, the scaling depends also on impactor geometry and velocity. Given that, an optimum value can be determined with equity of boundary conditions and the solution that maximize absorption should be evaluated case by case.

Fig. 5 shows the results for the same analysis on the value of static (μ_S) and dynamic (μ_D) coefficient of friction: the performance increases with the increase of the two coefficients. The influence is lower than interface parameter, mostly for two reasons: first, friction arises only after that delamination occurs; second, it plays a role only for the sliding component of the interface displacements. Friction mainly arises from surface morphology. Since the morphology affects in some measure also the interface strength and given the uncertainty in the experimental measuring of these friction coefficients, friction could be considered in some way a minor amount of contribute to the shear interface strength, and its effect neglected.

4. Oblique impact

Simulations of 15°, 30°, 45°, 60° oblique impact were performed and compared with normal impactor incidence. The initial velocity of the impactor, for all cases, is 700 m/s. The impactor is assumed at this stage to be rigid. In general, the ballistic limit of the target tends to increase with the increase in angle of obliquity, since, from geometrical consideration the length of the impactor path within the target would be greater in the case of oblique impact (Fig. 6). In case of inclined target the projectile imprint on the plate tends to be elliptical with one of the two axes that increase its length with the projectile obliquity, as also confirmed by our numerical simulations (Fig. 7). From Heteringhton and Rajagopalan[30], the expression that defines for the i-th layer the amount of the absorbed energy in the Eq. (3) can be updated, for geometric considerations, as follows:

$$E_{abs}(\beta;\theta) = \sigma_i \pi c_i d_i t_i \tag{7}$$

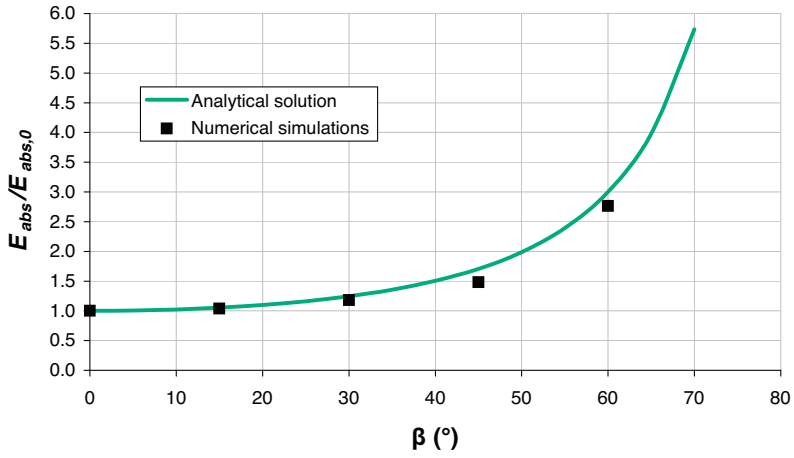

Fig. 8. Variation of panel energy absorption with the angle of impact incidence β. Energy values are normalized with respect to the absorbed value in case of normal impact($E_{abs,0}$). Numerical simulations results are compared with the ones from the analytical relation proposed by Hetherington,[13] assuming the opening angle of the cone $\theta = 45^\circ$.

where β is the incidence angle of the impactor, θ is the angle of diffusion of deformation after impact according to Fig. 7, c_i and d_i the axes of the imprint ellipse given for each layer by (Fig. 7):

$$c_i = \frac{R}{\cos\,\beta} + \sum_{i=1}^{n} t_i\,\tan\theta \tag{8.a}$$

$$d_i = R + \sum_{i=1}^{n} t_i\,\tan\theta \tag{8.b}$$

Fig. 8 shows the variation of absorbed energy with different angle of incidence, and θ assumed to be 45°. The values are normalized with respect to the energy absorbed under normal impact condition. The results from numerical simulations are in good agreement with the analytical model, although the latter is based on very simple hypotheses. The difference seems to slightly increase with the angle of incidence, and this can be explained by the fact that with the increase of obliquity the real behaviour tends to diverge with respect to the geometric assumptions of the conoid formation. We underline the similarity with trend provided in Iqbal et al.[31] which performed simulations and experiments on metallic targets.

Another important aspect in oblique impact is the projectile axis obliquity variation with respect to its original configuration. This is a direct consequence of the non-symmetry given by the initial incidence itself. Depending both on the nature of the target and the shape of the projectile, this variation can be positive, i.e. increases original obliquity (measured as the angle between the normal to the target and the projectile axis, Fig. 7), or negative. Fig. 9 shows the trend of the obliquity variation in relation to the initial inclination of the trajectory: the numerical spots can be fitted with a quadratic function and the obtained results can be correlated with the analytical previsions provided in Rajagopal et al.[32] for solely composite targets. Notice that for the specific set of simulations performed, in particular for the used impactor geometry and the specific plate stacking sequence, the variation of obliquity is negative: the projectile, instead of being driven and incorporated in the thickness, assuring a further mechanism of protection, is accommodated to the backing. This behaviour can be explained both with the specific target material behaviour

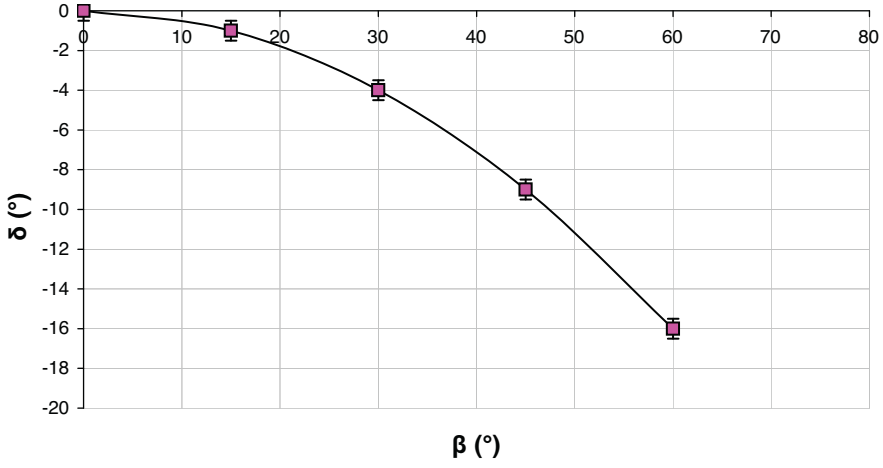

Fig. 9. Variation of projectile obliquity δ with the initial angle of impact incidence β. The negative sign of δ means that the impactor tends to realign along the normal direction, enhancing its penetrability.

under high-strain compressive loads and the peculiar shape of the projectile faces, which helps the penetration instead of driving the impactor within layers. This suggests further investigation on how these can affect the sign of variation of obliquity, which means to discriminate between a high perforating striker or not, simply by changing the layer stack-up or the projectile shape. The combined effect of target obliquity and projectile shape as performed in Iqbal et al.[30] for thin steel targets will be extended to composite and ceramic-composite targets in a subsequent paper.

5. Conclusions

Finite element models of ceramic-composite panels under normal and oblique impact were developed. Our computations demonstrate good agreement with existing experimental data and the prevision of analytical models: thus, we can conclude that these simulations can be used for an improved design of lightweight ceramic-composite protective panels. We showed that the energy absorption of the plate can be maximized for each configuration by setting proper interface parameter: the best behaviour is not given simply by the case of maximum delamination area but from the combination of material fracture, dissipation through deformation of the plate apart from the projectile imprint, and vibrations. Since the impactor penetrability (related to its velocity, geometry, and mass), the laminate stacking sequence, and the material constitutive law can affect the overall response, general values of these parameters cannot be provided. However, numerical simulations configure as a powerful tool to gain case by case the absorption optimum, maximizing the contribution in adding further layers, saving then in weight. Finally, oblique impact was observed to cause interesting effect on variation of striker obliquity, suggesting further investigation on this direction, in order to understand, for example, the best arrangement of ceramic and composite components, the worst shape condition in terms of projectile penetration, and to explain the optimized structure of natural dermal armour.

Acknowledgments

NMP is supported by the European Research Council (ERC StG Ideas 2011 BIHSNAM on “Bio-Inspired hierarchical super-nanomaterials”, ERC PoC 2013-1 REPLICA2 on “Large-area replication of biological anti-adhesive nanosurfaces”, ERC PoC 2013-2 KNOTOUGH on “Super-tough knotted fibres”) and European Commission under Graphene Flagship.

References

1. Pugno NM. Mimicking nacre with super-nanotubes for producing optimized super-composites. *Nanotechnology* 2006;**17**:5480–4.
2. Pugno NM. Graded cross-links for stronger nanomaterials – Insight. *Mater Today* 2010;**13**:40–3.
3. Tan PH, Han WP, Zhao WJ, Wu ZH, Chang K, Wang H, et al. The shear mode of multi-layer graphene. *Nat Mater* 2012;**11**:294–300.
4. Pugno NM. *The egg of Columbus for making the world’s toughest fibres*; 2013 (available at arXiv:1304.6658).
5. *Simple trick turns commercial polymer into world’s toughest fiber*. MIT Technology Review; May/June 2013.
6. Yang W, Chen IH, Gludovatz B, Zimmermann EA, Ritchie RO, Meyers MA. Natural flexible dermal armor. *Adv Mater* 2013;**25**:31–48.
7. *DSM Dyneema*; 2013. http://www.dyneema.com
8. *TEIJIN Aramid*; 2013. http://www.teijinaramid.com/aramids/twaron/
9. Cunniff PM. Dimensionless parameters for optimization of textile-based body armor systems. In: *Proceedings of the 18th international symposium on ballistics*. 1999. p. 1303–10.
10. Recht RF, Ipson TW. Ballistic perforation dynamics. *J Appl Mech* 1963;**30**(3):384–90.
11. Abrate S. Ballistic Impact on Composites. In: *16th international conference on composite materials*. 2007.
12. Espinosa HD, Dwivedi S, Zavatteri PD, Yuan G. A numerical investigation of penetration in multilayered material/structure system. *Int J Solids Struct* 1997;**35**(22):2975–3001.
13. Hetherington JG, Lemieux PF. The effect of obliquity on the ballistic performance of two component composite armours. *Int J Impact Eng* 1994;**15**:133–7.
14. Sadanandan S, Hetherington JG. Characterisation of ceramic/steel and ceramic/aluminium armours subjected to oblique impact. *Int J Impact Eng* 1997;**19**:811–9.
15. Abrate S. *Impact on composite structures*. Cambridge, UK: Cambridge University Press; 1998.
16. Abrate S. Modeling of impacts on composite structures. *Compos Struct* 2001;**51**:129–38.
17. Abrate S. *Impact engineering of composite structures, CISM courses and lectures*, vol. 526. New York: Springer Wien; 2011.
18. Goldsmith W. *Impact – the theory and phisical behaviour of colliding solids*. Mineola, New York: Dover; 2001.
19. Ben-Dour G, Dubinsky A, Elperin T. High-Speed penetration modeling and shape optimization of the projectile penetrating. *Mech Based Des Struct* 2009;**37**:538–49.
20. Banichuk NV, Ivanova SY, Makeyev YV. On penetration of rigid non-axisymmetric bodies into elastic-plastic medium. *Probl Strength Plast* 2010;**70**:131–9.
21. Forrestal MJ, Altman BS, Cargile JD, Hanchak SJ. An empirical equation for penetration depth of ogive-nose projectiles into concrete targets. *Int J Impact Eng* 1994;**15**:395–405.
22. Forrestal MJ, Tzou DY. A spherical cavity-expansion penetration model for concrete targets. *Int J Solids Struct* 1997;**34**:4127–46.
23. Jacobs MJL, Van Dingenen JLJ. Ballistic protection mechanisms in personal armour. *J Mater Sci* 2001;**36**(3127):3142.
24. Hallquist JO. *LS-DYNA theory manual*. Livermore: Livermore Software Technology Corporation; 2006.
25. Hallquist JO. *LS-DYNA keyword user’s manual*. Livermore: Livermore Software Technology Corporation; 2006.
26. Hetherington JG. The optimization of two components composite armours. *Int J Impact Eng* 1992;**12**:409–14.
27. Cronin DS, Bui K, Kauffmann C, McIntosh G, Berstad T. Implementation and validation of the Johnson–Holmquist ceramic material model in Ls-Dyna. In: *4th European LS-DYNA users conference*. 2003.
28. Johnson GR, Holmquist TJ. Response of boron carbide subjected to large strain, high strain rates, and high pressures. *JPN J Appl Phys* 1999;**85**(12):8060.
29. Schweizerhof K, Weimar K, Münz T, Rottner T. Crashworthiness Analysis with Enhanced Composite Material Models in LS-DYNA, Merits and Limits. In: *LS-DYNA world conference*. 1996.
30. Hetherington JG, Rajagopalan BP. Investigation into the energy absorbed during ballistic perforation of composite armours. *Int J Impact Eng* 1994;**11**(1):33–40.
31. Iqbal MA, Diwakar A, Rayput A, Gupta NK. Influence of projectile shape and incidence angle on the ballistic limit and failure mechanism of thick shell plates. *Theor Appl Fract Mech* 2012;**62**:40–53.
32. Rajagopal A, Naik NK. Oblique ballistic impact behaviour of composites. *Int J Damage Mech* 2013;**0**(0):1–29.